Microstructural Assessment of Nitrogen-Strengthened Austenitic Stainless-Steel Welds Using Thermoelectric Power

A.N. LASSEIGNE, D.L. OLSON, H.-J. KLEEBE, and T. BOELLINGHAUS

The electronic properties of an alloy correlate directly to its microstructure. The thermoelectric power coefficient has been determined in this investigation to be a rapid and accurate measurement that can be used for microstructural assessment and correlated to achieve the maximum material performance of structural alloys. In high-nitrogen-strengthened stainless-steel welds, nitrogen partitions into solid-solution nitrogen and nitrides during the welding thermal cycle. The formation of nitrides results in a degradation of the mechanical properties and the corrosion resistance. Thermoelectric power measurements offer a means of assessing the weld-interstitial nitrogen content, which allows for a better correlation between the nitrogen content and the weld-metal microstructure and properties. Using pressure-composition-temperature (PCT) (activity) diagrams, thermodynamic models are developed to describe the relationship between the thermoelectric power coefficient as a function of the interstitial nitrogen content and the formed nitride content. These correlations between the electronic property measurements and the interstitial nitrogen content will allow for a faster, nondestructive, and improved property prediction of nitrogen-strengthened stainless steels.

I. INTRODUCTION

THE electronic properties of an alloy correlate directly to its microstructure. This investigation studies the behavior of the correlation between the thermoelectric power coefficient and the interstitial nitrogen content associated with the weld microstructure. The thermoelectric power coefficient is sensitive to microstructural changes and will be demonstrated on nitrogen-strengthened austenitic stainless-steel welds.

Austenitic stainless steels are being strengthened with high levels of nitrogen for the enhancement of mechanical properties and corrosion resistance.[1,2] Austenitic stainless steel has a high solubility for nitrogen; however, in particular alloys, the solubility of the nitrogen decreases with increasing temperature. During the welding of nitrogen-strengthened stainless steel, the solubility of nitrogen can become exceeded, resulting in the partitioning of nitrogen on cooling into solid-solution nitrogen and nitrides. If the microstructure and the properties are to be properly correlated, it is essential that both the solid-solution nitrogen and the nitride-nitrogen contents be easily and rapidly determined. In this investigation, electronic properties are used to develop insight into the nature and role of nitrogen in these nitrogen-strengthened stainless steels.

Thermoelectric Power

To gauge the magnitude of the influence of the soluble nitrogen relative to the nitride nitrogen, the thermoelectric power coefficient, also referred to as the Seebeck coefficient, is introduced. The thermoelectric power coefficient, Z, is a temperature-dependent electronic property of the material that can be described as the entropy of the free electrons in the alloy. Given the voltage difference, ΔV, between two points held at a constant temperature difference, ΔT, on the specimen surface, the thermoelectric power coefficient can be determined using the mathematical expression:

$$Z = \frac{\Delta V}{\Delta T} + Z_{\text{ref}} \qquad [1]$$

where Z_{ref} is the thermoelectric power coefficient of the reference material, which in this investigation is a tungsten tip in contact with the specimen surface. A schematic diagram of the thermoelectric power measurement setup is shown in Figure 1.

From solid-state electronic models, the thermoelectric power coefficient is a function of the electron concentration, the effective mass of the electron, and the electronic scattering behavior in an alloy, which are all influenced by the solute content, lattice strain, microstructural changes, material processing, and time-dependent phase changes. As the nitrogen content changes in the austenitic stainless steel, there is a resulting change in the thermoelectric power coefficient, thus making it a valued property for the solute content and microstructural assessment.

In metallic alloys, the value and the sign of the thermoelectric power coefficient depends on the features of the electronic bands in the vicinity of the Fermi energy level, which can be seen on a plot of the density of electronic states.[3,4,5] In turn, the Fermi energy surface in k-space changes with the electronic filling in the conduction band, due to the electron donation by the solute nitrogen atoms.[1] Also, the nitrogen atoms strain the lattice and cause changes in the d-electron overlap of the transition metal atoms, resulting in the decreased action of the Pauli-exclusion principle, which

A.N. LASSEIGNE, Graduate Research Scientist, and D.L. OLSON and H.-J. KLEEBE, Professors, are with the Department of Metallurgical and Material Engineering, Colorado School of Mines, Golden, CO 80401. Contact e-mail: alasseig@mines.edu T. BOELLINGHAUS, Vice President, is with the Federal Institute of Materials Research and Testing, Berlin, Germany 12205.

Manuscript submitted February 4, 2005.

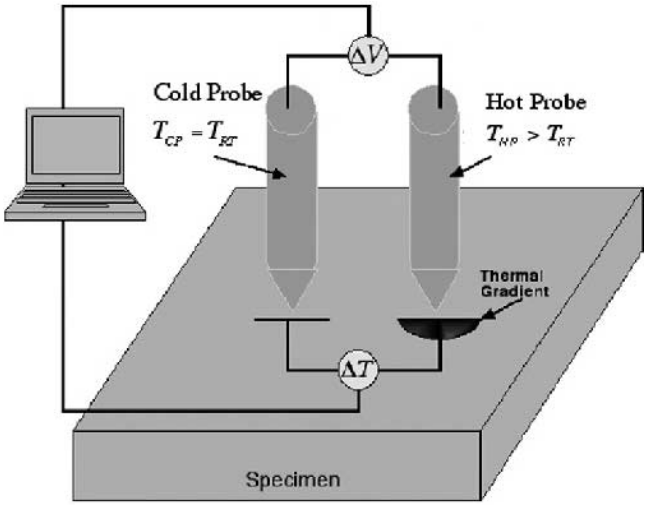

Fig. 1—Schematic representation of the probe thermoelectric power device.

should change the shape of the *d*-band. Using the example of a solid solution, with the high degeneracy of the free-electron gas useful in understanding the dependent variables, the resulting thermoelectric power coefficient, *Z*, is related to the electron theory through the following expression:

$$Z = \left(\pm\frac{\bar{k}}{e}\right)(27.1)\left(r + \frac{3}{2}\right)\left(\frac{m_e}{h^2}\right)\left(\bar{k}\,Tn^{\left(-\frac{2}{3}\right)}\right) \qquad [2]$$

where *r* is the electron-scattering parameter determined by the dominating scattering mechanism, *h* is Planck's constant, $\bar{k}$ is Boltzmann's constant, *n* is the electron concentration, *e* is the electronic charge, *T* is the temperature, and m_e is the effective mass. From the free-electron model, the electron concentration is directly related to the Fermi energy. The effective mass describes the rate at which the energy states are filled in *k*-space at the Fermi energy level, with an increasing electron concentration.[3,4,5] The effective mass can be described as

$$m_e = \hbar^2\left(\frac{d^2E}{d\mathbf{k}^2}\right)^{-1}_{E=E_F} \qquad [3]$$

where **k** is the wave vector and $\hbar$ is Planck's constant *h* divided by 2π. The effective mass, m_e, describes the shape of the *s*-, *p*-, and *d*-bands that are in contact with the Fermi energy level. The shape of the bands at the contact position offers a sensitive indication of changes in alloy composition, phase content, and lattice strain.

II. EXPERIMENTAL PROCEDURE

The nitrogen-strengthened alloy 1.4565 (AISI 34565) has been developed for applications in high-chloride environments such as seawater, and has been used for this investigation. The chemical composition of the stainless-steel alloy 1.4565 (AISI 34565) is given in Table I, where it is important to notice that this alloy has been strengthened with a nitrogen content of 0.458 wt pct, which results in a yield strength of approximately 60 ksi (420 MPa). High levels of nitrogen stabilize the austenitic phase, increase strength, and increase pitting and crevice corrosion resistance.[1,2,6]

Table I. Alloy 1.4565 (AISI 34565) Nominal Chemical Composition (Weight Percent)

C	Si	Mn	P	S	Cr	Ni	Mo
0.028	0.182	6.080	0.017	<0.001	23.82	18.83	5.639
Ti	Nb	N	Cu	Al	Ta	Fe	—
0.017	0.028	0.458	0.104	0.015	0.011	44.78	—

Table II. Plasma Arc Welding Parameters for Alloy 1.4565 (AISI 34565)

Weld travel speed	20 cm/min
Current	190 A
Voltage	15 V
Nitrogen flow rate	4 L/min
Argon flow rate	15 L/min
Plasma flow rate	2 L/min
Arc length	6 mm
Electrode diameter	4 mm

Autogenous plasma arc welds in a nonkeyhole mode were made on 12.5-mm-thick (1/2-in.) plates of the stainless-steel alloy 1.4565 (AISI 34565), using a shielding-gas mixture of Ar-20 pct N_2, with the welding parameters given in Table II. Variation in the number of weld passes (or number of weld beads) was used to achieve a systematic increase in the total nitrogen content, due to the nitrogen pickup from the nitrogen-rich argon-shielding gas.

The weld specimens were analyzed for both their chemical and microstructural constitution. In this investigation, the microstructure is characterized relative to both the interstitial nitrogen and the nitride contents. The interstitial nitrogen contents are determined through the combined utilization of the Beeghly ester-halogen digestion method[7,8,9] and the LECO* Nitrogen Determinator, which are thoroughly described in the following references. The microstructure was characterized using a JEOL* JXA-840 scanning electron microscope (SEM).

*LECO is a trademark of LECO Corporation, St. Joseph, MI.

*JEOL is a trademark of Japan Electron Optics Ltd., Tokyo.

The thermoelectric power coefficient was the electronic measurement used to assess the nature and role of the nitrogen content in nitrogen-strengthened stainless-steel weldments. A schematic diagram of the thermoelectric power measurement setup was shown in Figure 1. The Seebeck apparatus was designed to allow the copper probes with tungsten contact tips to apply a constant pressure to a surface, while completing temperature and voltage measurements. The constant pressure was achieved by applying a constant load on top of the probe-spring arrangement. The Seebeck apparatus measures the thermoelectric power coefficient by applying a hot copper probe with a tungsten contact tip in the center of the weld, and a cold copper probe with a tungsten contact tip (a 10 °C temperature difference) in the base metal, as shown in Figures 2(a) and (b). The 10 °C temperature difference (±0.1 °C) was accurately controlled by two Watlow temperature controllers (St. Louis, MO) and readouts, along with two type K thermocouples and two type T thermocouples; the potential measurements (±10 nV) were

made with a Keithley nanovoltmeter 2182 (Cleveland, OH). The actual thermoelectric power measurement occurs under the hot-probe tungsten contact tip. Seebeck measurements were performed on different surfaces, to determine the effect of the surface preparation. Seebeck measurements were performed on the as-welded fusion zone; the weldment was then milled down to remove any carburization layer; and the Seebeck measurement was remeasured. The Seebeck measurements for the as-welded condition and the milled condition are identical.

The tungsten contact tip of the copper probe has a diameter of approximately 381 μm. The depth of the thermal gradient under the hot tip is on the order of the diameter of the tungsten contact tip. Seebeck measurements can be made on uneven surfaces, which are often exhibited in weldments. On an uneven surface, the complete contact of the entire probe on the surface does not occur. The amount of contact is not an issue, because the nanovoltmeter has very high impedance, which significantly reduces the current, thus making the Seebeck measurement a potentiostatic measurement. The Seebeck measurement takes approximately 30 seconds to guarantee an accurate thermal distribution or voltage difference.

(*a*)

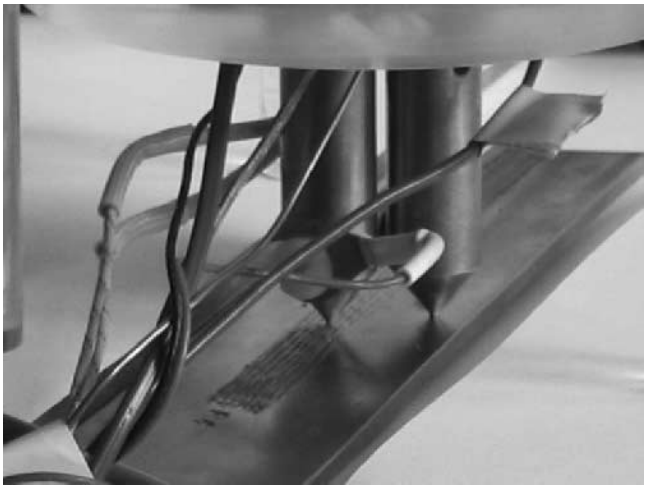

(*b*)

Fig. 2—(*a*) and (*b*) Thermoelectric-power-probe measuring device for austenitic stainless-steel weldments.

III. RESULTS AND DISCUSSION

The resulting autogenously welded microstructure of the alloy 1.4565 (AISI 34565) is shown in Figure 3, with an interstitial nitrogen content of 0.469 wt pct (0.551 wt pct total nitrogen). From the scanning electron micrograph, it is observed that there is an austenite-cored dendritic microstructure. Coring also denotes that there can be variations in mechanical properties and corrosion resistance.

Coring is normally caused by the partitioning of the solute on cooling through a two-phase field. The nature and amount of elemental partitioning is dependent upon the alloy solute contents, the solute partitioning coefficient, k, and the thermal experience during solidification.[12] The equilibrium partition coefficient is

$$k = \frac{C_S}{C_L} \qquad [4]$$

where C_s is the solute concentration at the constant temperature and pressure of the solidus, and C_L is the solute concentration, at the same constant temperature and pressure of the liquidus. The equilibrium partition coefficient controls the direction and extent of the segregation during solidification. Microsegregation during solidification results in an increase in the concentration of alloying elements, precipitates (carbides, nitrides, and intermetallic phases), and possibly porosity in the interdendritic liquid. Predicting from the iron-nitrogen phase diagram in Figure 4, and assuming

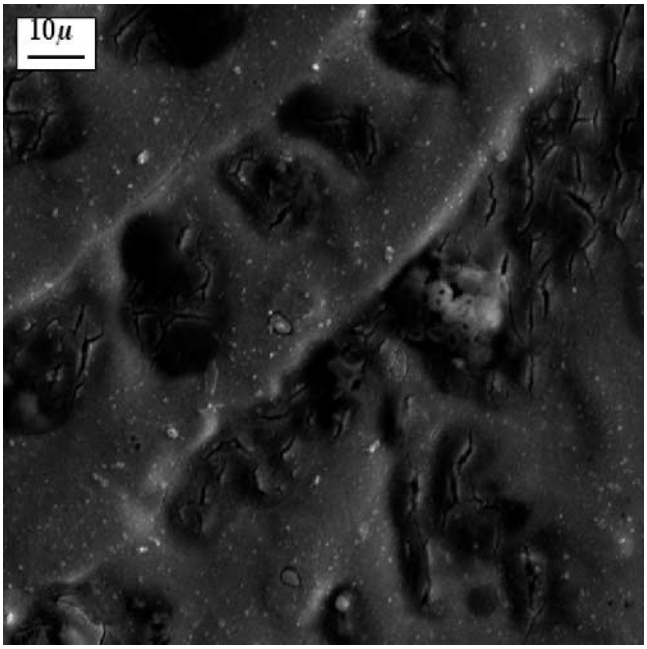

Fig. 3—SEM images at 2000 times magnification, for the plasma-welded stainless-steel alloy 1.4565 (AISI 34565) at the interstitial nitrogen content of 0.487 wt pct.

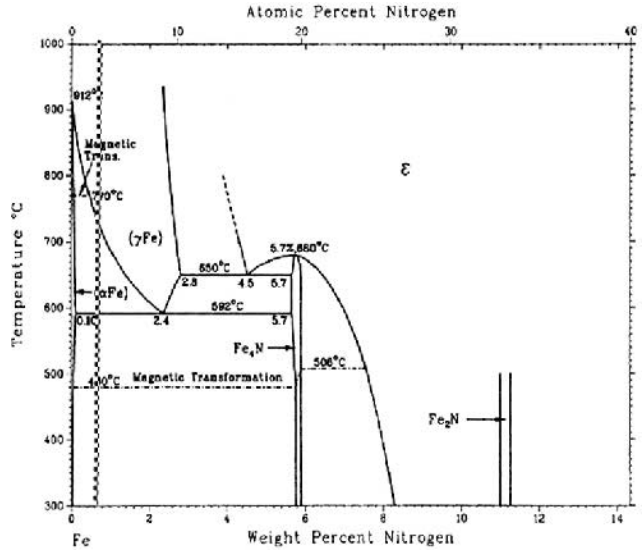

Fig. 4—Fe-N equilibrium diagram.[13]

that the extended phase lines on the diagram move up and to the left, a peritectic reaction similar to the iron-carbon system is expected.[13] Hence, from Figure 4, it can be concluded that the natural tendency is for the partition coefficient to be less than one ($k < 1$), so that nitrogen gets rejected into the liquid interdendritic region during solidification.[12,14,15]

Because the diffusion coefficient of nitrogen is orders of magnitude above that of the substitutional alloying elements, nitrogen is normally not prone to significant microsegregation, due to sufficient in-process homogenization.[1] However, as reported by Gavriljuk and Berns,[1] as the substitutional alloying elements begin to partition between austenite and ferrite stabilizers, nitrogen segregates to areas with higher nitride forming elements, such as chromium, manganese, and molybdenum contents, while the nitrogen is only partially depleted from the areas with the higher nickel, cobalt, and carbon content. During plasma arc welding, the moving solid-liquid interface may reject nitrogen, and there may be insufficient time for the nitrogen diffusion to achieve in-process homogenization. Because the nitrogen partitioned into the interdendritic region, it becomes supersaturated in the interdendritic region, resulting in nitride formation on cooling.

From the SEM image in Figure 3, the first weld pass shows a primary austenite dendritic solidification at places where there are small amounts of nitrides (≈15 pct formed nitrides) in the interdendritic region. As subsequent weld passes are made, more nitrogen is absorbed, which adds to the interstitial nitrogen content in the interdendritic region; the interstitial nitrogen increases in the interdendritic region, which results in supersaturated interstitial nitrogen, and thus the formation of more nitrides (≈20 pct formed nitrides). From the combined effort of energy-dispersive X-ray (EDX) analysis for elemental distribution (Figure 5) along with X-ray diffraction (XRD) (Figure 6), there is an indication that the formation of chromium nitrides in the interdendritic region may result in a susceptibility for sensitization, due to chromium depletion adjacent to the nitrides, thus increasing the importance of the characterization of the interstitial nitrogen content in nitrogen-strengthened stainless-steel weldments.

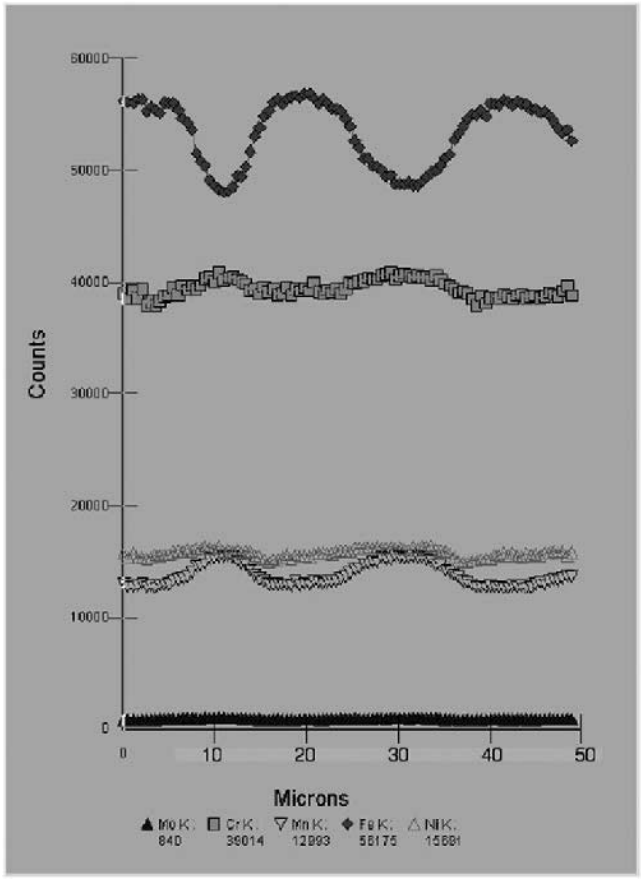

Fig. 5—EDX analysis of the plasma-welded stainless-steel alloy 1.4565 (AISI 34565).

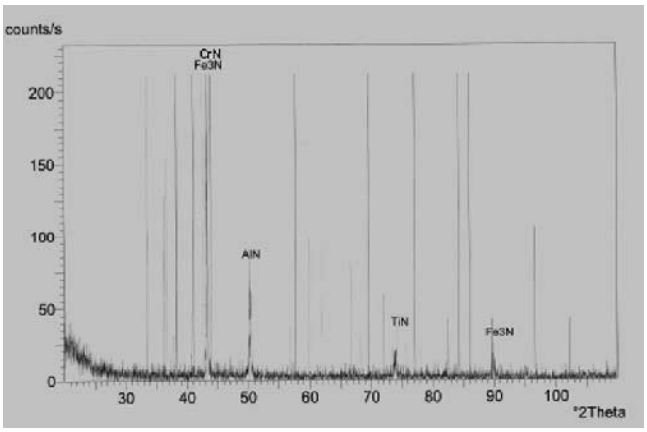

Fig. 6—XRD scan of the plasma-welded (triple-pass) stainless-steel alloy 1.4565 (AISI 34565).

The EDX line scan (Figure 5) shows that the solute composition across the weld metal has an approximate sinusoidal profile, due to coring. One way of expressing the degree of austenite stability in cored materials, such as weld metal, is to assume a sinusoidal distribution function, which can be applied to each of the segregating elements, as shown for iron in Figure 7.[14] The positive portion of the sinusoidal curve represents the interdendritic region, while the negative portion of the sinusoidal curve represents the dendritic region, as shown in Figure 8. It is assumed here that the

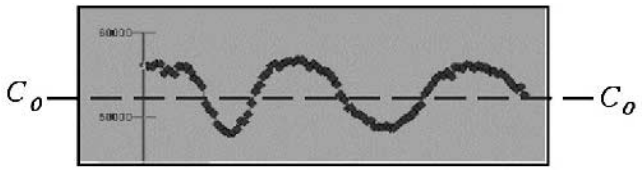

Fig. 7—Section of the EDX scan (Fig. 5) showing the average solute composition of the transverse section across the dendrite and the interdendritic region.

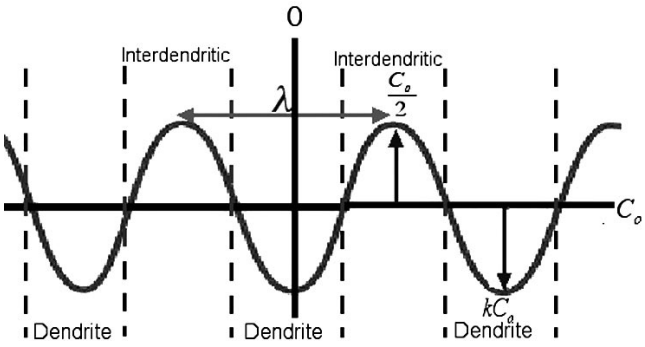

Fig. 8—Sinusoidal illustration of the microstructure composition, showing the dendritic and the interdendritic region.

average dendritic composition of the solute is similar to the base metal, and that all nitrogen in the dendritic region is in solid solution. The composition of nitrogen left behind the solid-liquid interface is $C_o k$, and is assumed to represent the minimum of the dendritic region as indicated in Figure 8. The $C_o k$ is the composition of nitrogen in the core of the dendritic region, assuming that C_o/k describes the amplitude of the interdendritic portion of the sinusoidal curve (Figure 8). A Fourier cosine series can be used to determine the nitrogen composition in the dendritic region, given as

$$C_{\text{dendrite}} = C_o - \frac{2kC_o}{\lambda}\int_0^{\lambda/4} -\cos\left(\frac{2\pi x}{\lambda}\right)dx \qquad [5]$$

Solving and simplifying Eq. [5] gives

$$C_{\text{dendrite}} = C_o\left(1 - \frac{k}{\pi}\right) \qquad [6]$$

The average composition of the solute in the dendrite is just a fraction smaller than the average composition of the microstructure, as shown in a section of the composition sinusoid for the solute in the stainless-steel alloy 1.4565 (AISI 34565) (Figure 7).

A. *Thermodynamic Stability of Nitrogen in the Stainless-Steel Alloy 1.4565 (AISI 34565)*

The solid-solution solubility of nitrogen in stainless-steel alloy 1.4565 (AISI 34565) has been calculated from the Wada and Pehlke[16] equations, and is shown in Figure 9. Unexpectedly, the solubility of nitrogen decreases with increasing temperature, which means that the solution exhibits exothermic behavior.[17] Exothermic behavior suggests a compound formation such as nitrides. In the following, the

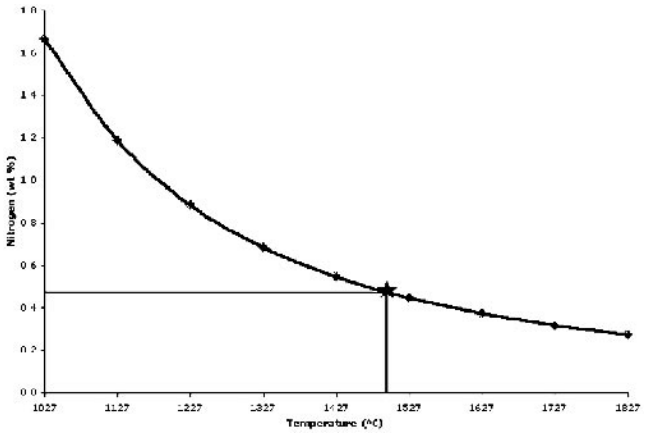

Fig. 9—Nitrogen content as a function of temperature, from the Wada and Pehlke calculation for the solubility of nitrogen in the nitrogen-strengthened austenitic stainless-free-steel alloy 1.4565 (AISI 34565).[16]

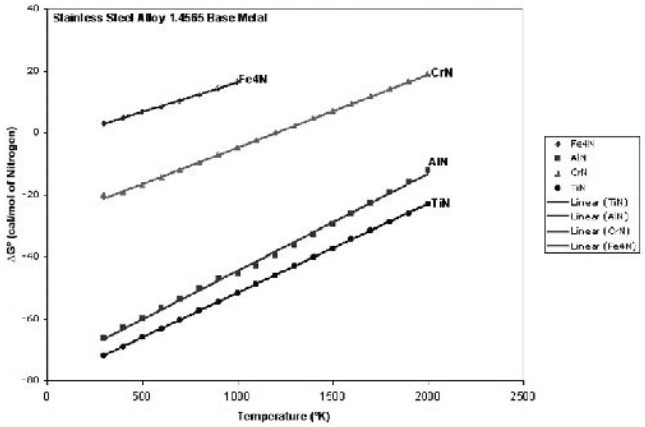

Fig. 10—Ellingham–Richardson diagram, modified to take into account the alloying elements in the stainless-steel alloy 1.4565 (AISI 34565) and in the welded stainless-steel alloy 1.4565 (AISI 34565) (dashed lines).

nitrogen solubility and nitride formation is modeled, based on thermodynamic predictions.

The Ellingham–Richardson diagram plots the change in the standard free energy of formation as a function of temperature for carbides, oxides, nitrides, *etc*., giving useful information about the order of nitride formations. The nitride standard free energies given in the Ellingham–Richardson diagram are customized to take into account each alloying addition in the stainless-steel alloy 1.4565 (AISI 34565), through the utilization of the Wada and Pehlke equation for the activity of nitrogen, as shown in Figure 10.[18] Figure 10 is a plot of the free energy of formation of the nitrides as a function of temperature, for the stainless-steel alloy 1.4565 (AISI 34565) base metal. All thermodynamic data came from Pankratz and Elliot.[19,20,21]

Figure 10 indicates that, thermodynamically, the first nitrides to form are titanium nitride and aluminum nitride. The aluminum and titanium quickly become exhausted, which leads to the formation of chromium nitrides and iron nitrides. The nitrides are present in the interdendritic region, due to the supersaturation of the nitrogen in this region. Iron nitride (Fe_3N) forms in the stainless-steel alloy 1.4565 (AISI 34565) welds, as determined by XRD, shown earlier in

Figure 6. However, thermodynamic data were not available for the Fe_3N iron nitride phase, for thermodynamic calculations. When examining the iron-nitrogen phase diagram (Figure 4), the Fe_3N phase is the ε-phase.

Notice that from the Ellingham–Richardson diagram, the positive standard free energy of iron nitride (Fe_4N), as compared to the negative free energies of aluminum nitride and titanium nitride. It would be suspected that Fe_4N would never form, due to the location on the Ellingham–Richardson diagram (positive free energy), and Fe_3N must exhibit a negative standard free energy.

B. *Thermoelectric Power and Nitrogen Correlations*

The thermoelectric power coefficient was determined for all welds and correlated to the total nitrogen and interstitial nitrogen content. The thermoelectric power coefficient as a function of total nitrogen is plotted in Figure 11. In Figure 12, the thermoelectric power coefficient is plotted as a function of the interstitial nitrogen content, revealing a linear relationship. As the interstitial nitrogen content is decreased,

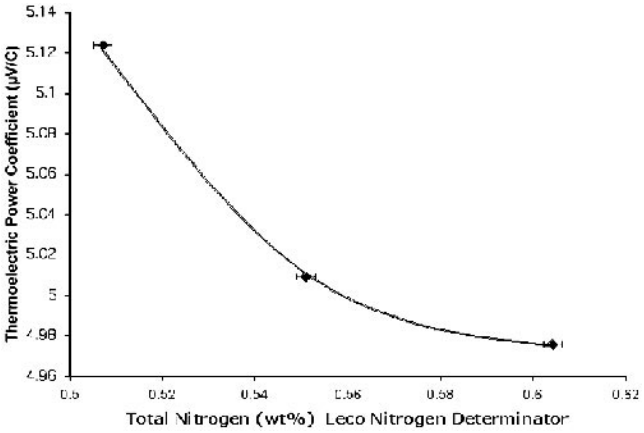

Fig. 11—Thermoelectric power as a function of the total nitrogen content for the plasma-welded stainless-steel alloy 1.4565 (AISI 34565), with argon-20 pct nitrogen shielding gas.

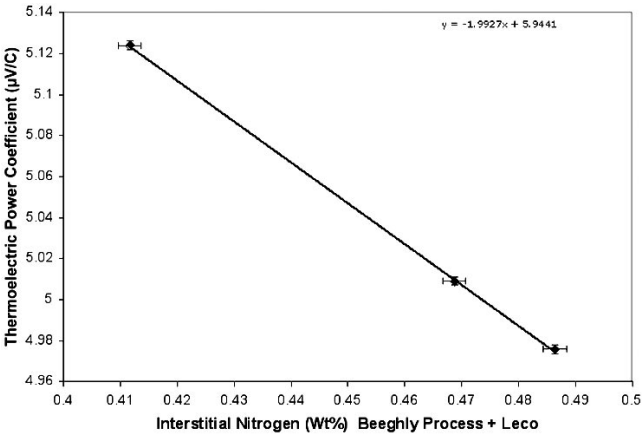

Fig. 12—Thermoelectric power as a function of the interstitial nitrogen content for the plasma-welded stainless-steel alloy 1.4565 (AISI 34565), with argon-20 pct nitrogen shielding gas.

due to the formation of nitrides, the thermoelectric power coefficient increases. The lattice strain due to nitrogen addition causes changes in the *d*-electron overlap between lattice transition atoms, which means a change in the extent of application of the Pauli-exclusion principle. This behavior changes the electronic effective mass and, thus, the thermoelectric power coefficient. In the following sections, thermodynamic models will be developed to describe the behavior shown in Figures 11 and 12.

C. *Thermodynamic Models*

A thermodynamic expression of equilibrium can be used to derive the relationship between the thermoelectric power coefficient and the activity of nitrogen. Beginning with the first law of thermodynamics and assuming a reversible process,

$$dE = TdS - PdV - \delta w_{\text{ext}} \quad [7]$$

where E is the internal energy, S is the entropy, T is the temperature, P is the pressure, V is the volume, and w_{ext} is the external work done by the system.

At constant pressure ($dP = 0$), enthalpy is introduced as the sum of the internal energy and the product of pressure and volume ($H = E + PV$). Differentiating enthalpy and incorporating into Eq. [7] gives

$$dH = TdS - \delta w_{\text{ext}} \quad [8]$$

Equation [8] is inserted into the differential Gibb's free energy ($dG = dH - SdT - TdS$) and is given as

$$dG = -\delta w_{\text{ext}} - SdT + \Sigma \mu_i n_i \quad [9]$$

where the $\Sigma \mu_i n_i$ is additional free energy, accounting for the addition of alloying elements to the solution, and μ_i is the chemical potential of species i.

The external work term is the product of the number of moles of transported electrons, Faraday's constant (96,487 Coulombs per electron equivalent), and the electric potential. The thermoelectric power coefficient involves the generation of an electric potential difference, ΔV, under an applied temperature difference, ΔT, given as

$$\Delta V = Z\Delta T \quad [10]$$

Under the assumption that the external work is electric work, by analogy to the thermodynamics of a reversible cell, the external work term becomes

$$\delta w_{\text{ext}} = -nF(Z\Delta T) \quad [11]$$

and Eq. [9] can be rearranged as

$$dG = nF(Z\Delta T) - SdT + \Sigma \mu_i n_i \quad [12]$$

where $\mu_i = \mu_i^o + RT \ln a$. Assuming equilibrium conditions, $\Delta G = 0$, and solving Eq. [12] for the thermoelectric power coefficient gives

$$Z = \frac{S}{nF} - \frac{\Sigma \mu_i n_i}{nF\Delta T} \quad [13]$$

Because the thermoelectric power coefficient measures a change, it is important to note that the reference-state thermoelectric

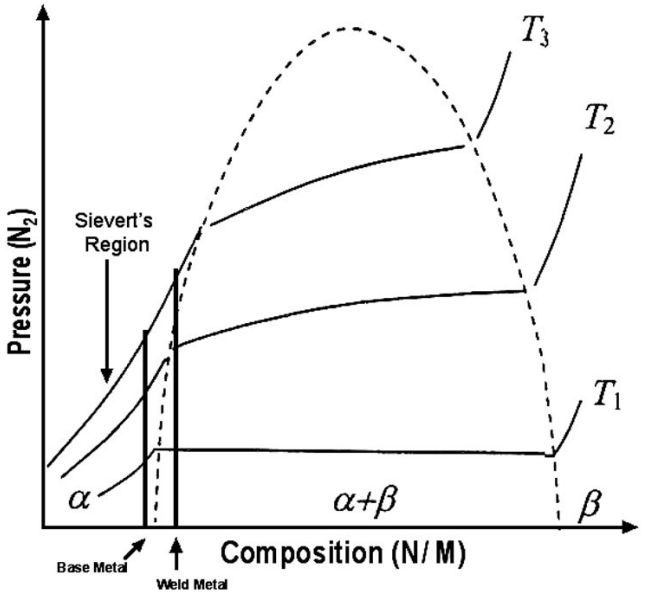

Fig. 13—Schematic PCT diagram for nitrogen, where the α-phase is interstitial nitrogen, the (α + β)-phase is interstitial nitrogen and nitrides, and the β-phase is nitride phase. The blue line indicates the location of the base metal, and the red line indicates the position of the weld metal.

power coefficient is a function of entropy before the addition of nitrogen, given as

$$Z^\circ = \frac{S}{nF} \qquad [14]$$

Then, when nitrogen is added to the metal, the thermoelectric power technique measures a change in the thermoelectric power coefficient, which is $\Delta Z = Z - Z^o$, so that the actual thermoelectric power coefficient measurement gives

$$\Delta Z = \frac{\Sigma \mu_i n_i}{nF\Delta T} \qquad [15]$$

Equation [15] is then considered for each region of the pressure-composition-temperature diagram (PCT) of metal and nitrogen, as shown in Figure 13. There are three different regions making up the PCT diagram: (1) the alpha-phase region, which is interstitial nitrogen; (2) the beta-phase region, which is formed nitrides; and (3) the (alpha + beta)-phase region, which is composed of both interstitial nitrogen and formed metal nitrides. It is important to determine the thermodynamic relationship between the thermoelectric power coefficient and the nitrogen content in the alpha-phase and beta-phase regions. With the knowledge of these two regions and the use of the rule-of-mixtures, the thermoelectric power coefficient for the (alpha + beta) two-phase region can be determined. In this investigation, the alpha-region and the (alpha + beta)-region are important, because the resulting solidified weld structure is made up of a dendritic region with interstitial nitrogen and an interdendritic region that consists of saturated interstitial nitrogen and formed nitrides.

D. *Alpha-Phase Region*

First, the alpha-phase region is considered (Figure 13), in which the appropriate reaction is given as

$$N_2(g) \rightarrow 2\underline{N}\,(M) \qquad [16]$$

The $\underline{N}$(M) is a nitrogen atom in solid solution in the metal matrix, M. The thermoelectric power coefficient for the alpha-phase region derived from Eq. [15] is

$$\Delta Z_\alpha = -\frac{\Delta G^\circ}{nF\Delta T} - \frac{RT}{nF\Delta T}\left(\ln [a_N]^2 - \ln [p_{N_2}]\right) \qquad [17]$$

E. *Beta-Phase Region*

The thermoelectric power coefficient must be determined in the beta-phase region (Figure 13) to develop an expression for the thermoelectric power coefficient for the (alpha + beta)-phase region. The reaction for the beta-phase region (nitride formation) is

$$\frac{2}{x}M + N_2(g) \rightarrow \frac{2}{x}MN_x \qquad [18]$$

The thermoelectric power coefficient, assuming the activity of the metal nitride and metal is equivalent to one ($a_M = 1$, $a_{MN} = 1$), is derived from Eq. [15] and is given as

$$\Delta Z_\beta = -\frac{\Delta G^\circ}{nF\Delta T} - \frac{RT}{nF\Delta T}\left(\ln [p_{N_2}]^{-1}\right) \qquad [19]$$

F. *(Alpha + Beta)-Phase Region*

In the (alpha + beta) two-phase region (Figure 13), there is the mixture between the alpha-phase of saturated nitrogen $X_{N(sat)}$ and the beta-phase at a fixed composition X_b, which forms a metal nitride MN_b. In this case, the rule-of-mixtures is used to give the thermoelectric power coefficient in the (alpha + beta) two-phase region as

$$\Delta Z_{\alpha+\beta} = (1 - Y)\left(-\frac{\Delta G^\circ}{nF\Delta T} - \frac{RT}{nF\Delta T}\ln\left(\frac{[a_N]^2}{[P_{N_2}]}\right)\right) + Y\left(-\frac{\Delta G^\circ}{nF\Delta T} - \frac{RT}{nF\Delta T}\ln [P_{N_2}]^{-1}\right) \qquad [20]$$

where Y is the fraction of beta-phase. Equation [20] can be simplified by using the constant A, which is given as

$$A = \left(-\frac{\Delta G^\circ}{nF\Delta T} - \frac{RT}{nF\Delta T}\ln\left(\frac{[a_N]^2}{[P_{N_2}]}\right)\right) \qquad [21]$$

and constant B is given as

$$B = \left(-\frac{\Delta G^\circ}{nF\Delta T} - \frac{RT}{nF\Delta T}\ln [P_{N_2}]^{-1}\right) \qquad [22]$$

so that the simplified version of Eq. [20] becomes

$$\Delta Z_{\alpha+\beta} = A + (A + BY) \qquad [23]$$

The relationship between the thermoelectric power coefficient and the activity of nitrogen in three regions is supported by similar experimental results for hydrogen solubility behavior in hydrogen storage material and structural steel from Park *et al.*,[3] Niyomsoan,[22] and Termsuksawad.[23]

Figure 14 is a schematic that illustrates the comparison between a PCT diagram and a thermoelectric power

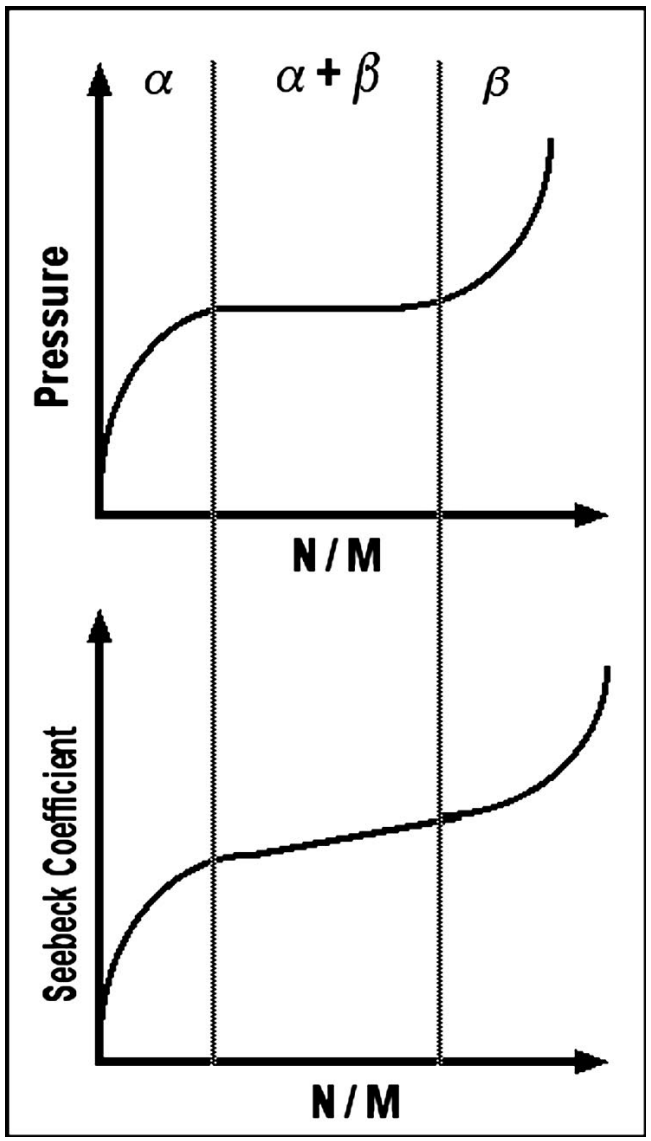

Fig. 14—Comparison of the pressure (chemical potential) and the Seebeck coefficient as a function of nitrogen for the α-phase, (α + β)-phase, and β-phase.

coefficient-composition temperature diagram. In the PCT diagram, the (alpha + beta)-region is isobaric, because the chemical potentials of alpha and beta are equal. In the thermoelectric power coefficient diagram, the (alpha + beta)-region is linear (not constant), which is consistent with Eq. [23]. The thermoelectric power coefficient represents the entropy of the electron in the alpha- and beta-phases, which can be subject to a rule-of-mixtures averaging having a slope across the two-phase (alpha + beta) region.

The thermoelectric surface contact probe has a diameter of 381 μm, which when compared to the SEM micrograph in Figure 3, suggests that the thermoelectric power coefficient is an average of the dendritic and interdendritic regions of the weld. So, to model the thermoelectric power coefficient of an austenitic stainless-steel weld, the model needs to describe the entire weld microstructure, including the dendritic region and the interdendritic region, as shown in Figure 15. On the PCT diagram, the weld composition is

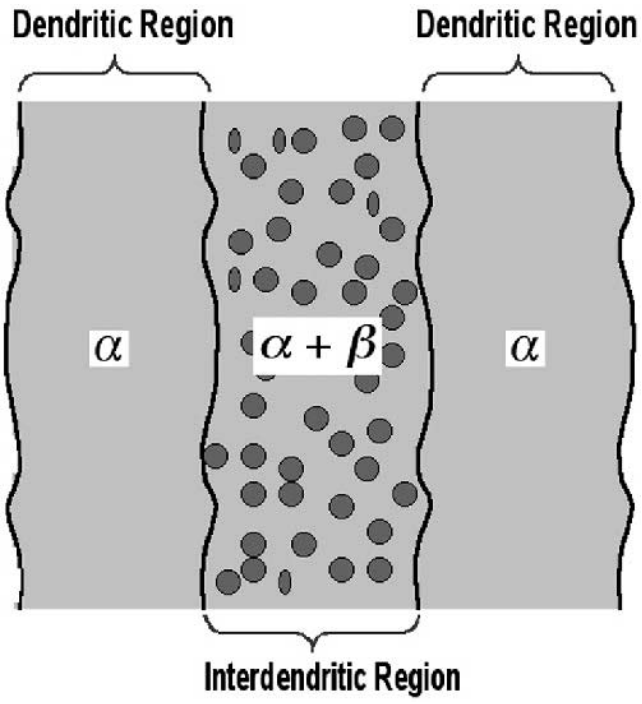

Fig. 15—Schematic illustration of weld-metal dendritic solidification, indicating the dendritic (α) and interdendritic (α + β) regions.

shifted further to the right into the (alpha + beta)-phase region, as shown in Figure 13.

The thermoelectric power coefficient in the interdendritic region can be modeled using the rule-of-mixtures for composites, assuming that the dendritic region is interstitial nitrogen (alpha) and the interdendritic region is both interstitial nitrogen and formed nitrides (alpha + beta). The rule-of-mixtures for composite structures is applied first for the weld microstructure (dendritic + interdendritic), given as

$$Z = Z_{\alpha} X_{\alpha} + Z_{\alpha'+\beta} X_{\alpha'+\beta} \quad [24]$$

where Z is the total thermoelectric power coefficient and Z_{α} is the coefficient of the bulk interstitial nitrogen content in the dendrite. The expression ($Z_{\alpha'+\beta}$) is the coefficient for the two-phase interdendritic region of interdendritic nitride and alpha-phase (interstitial nitrogen). The X_{α} is the fraction of the alpha-phase in the dendrite, and $X_{\alpha'+\beta}$ is the fraction of the interdendritic alpha- and beta-phase. The X_{α} in the dendrite and the $X_{\alpha'+\beta}$ in the interdendritic region can be obtained from the SEM micrograph from Figure 3. Assuming that the sum of the interdendritic nitrogen content and nitride content is equivalent to the total nitrogen content, it follows that

$$X_{\alpha'} + X_{\beta} = 1 \quad [25]$$

Rearranging Eq. [25] and inserting it into Eq. [24] gives the thermoelectric power coefficient of the microstructure as

$$Z = Z_{\alpha'+\beta} + X_{\alpha}\left(Z_{\alpha} - Z_{\alpha'+\beta}\right) \quad [26]$$

The rule-of-mixtures is reiterated to model the interdendritic region, in which it is assumed that the interstitial nitrogen in the dendrite is constant and $Z_{\alpha'}$ should change, due to the

supersaturation of the interstitial nitrogen in the interdendritic region; here, however, it is assumed to be constant $Z_{\alpha'} \cong Z_{\alpha}$. The rule-of-mixtures for the interdendritic region becomes

$$Z_{\alpha'+\beta} = Z_{\beta} + (Z_{\alpha} - Z_{\beta})X_{\alpha'} \quad [27]$$

where X_{α} is the fraction of the core region of the dendrite and is assumed to be approximately constant for the same plasma welding parameters. Substituting Eq. [27] into $Z_{\alpha'+\beta}$ from Eq. [26] and simplifying gives the thermoelectric power coefficient as

$$Z = \text{Const.} + (Z_{\alpha} - Z_{\beta})(1 - X_{\alpha})X_{\alpha'} \quad [28]$$

Equation [28] suggests that the thermoelectric power coefficient is solidification-microstructure dependent, and thus agrees with the linear relationship for the thermoelectric power coefficient as a function of the interstitial nitrogen content in the interdendritic region, as shown in Figure 12. Equation [28] is also consistent with the schematic drawing of the Seebeck coefficient as a function of the fraction of interstitial nitrogen in the interdendritic region for this system, as shown in Figure 14.

G. *Correlation of Models to Experiments*

The modification of the Ellingham–Richardson (Figure 10) diagram, accounting for the high nitrogen content and alloying elements present in the stainless-steel alloy 1.4565 (AISI 34565), showed the thermodynamic order of the formation of nitrides and is consistent with the results presented here.

The linear correlation of the thermoelectric power coefficient for the plasma-welded stainless-steel alloy 1.4565 (AISI 34565), as a function of the interstitial nitrogen content in the interdendritic region shown in Figure 12, is consistent with the proposed weld-metal-composite model. From this model, the contribution of the thermoelectric power coefficient for the dendritic region is approximately constant, thus making changes in the measured thermoelectric power coefficient primarily sensitive to interstitial nitrogen content changes in the interdendritic region. From the rule-of-mixtures, this interstitial nitrogen content variation in the interdendritic region results in the linear correlation shown in Figure 12.

IV. CONCLUSIONS

1. The nitrogen-strengthened austenitic stainless-steel alloy 1.4565 (AISI 34565) weld-metal microstructure was characterized for its microstructure and alloy content, through the use of EDX analysis and XRD, and through the correlation of those results with electronic property measurements.
2. A linear relationship exists between the thermoelectric power coefficient and the interstitial nitrogen content.
3. A composite model, based on thermodynamics and solidification microstructure, linearly correlated the thermoelectric power coefficient to the weld-metal interstitial nitrogen activity.
4. The thermoelectric power coefficient is very sensitive to microstructural changes, due to the nitrogen content; with careful correlation to standards, it can be used as a rapid, nondestructive technique to assess interstitial nitrogen content in nitrogen-strengthened austenitic stainless steels.

ACKNOWLEDGMENTS

The authors acknowledge and appreciate the research support of the United States Army Research Office, Federal Institute of Materials Research and Testing (Berlin), National Science Foundation, and the American Society of Non-Destructive Testing. We also extend our appreciation to Professor Victor Kaydanov, for his expertise in thermoelectric power assessment, and to Dr. Carl E. Cross, for metallurgical comments.

REFERENCES

1. V.G. Gavriljuk and H. Berns: *High Nitrogen Steels: Structure, Properties, Manufacture, and Applications*, Springer, Berlin, Germany, 1999, pp. 1-290.
2. J.W. Park, S. Rao, and H.S. Kwon: *Corrosion*, 2004, vol. 60 (12), pp. 1099-1103.
3. Y.D. Park, A.N. Lasseigne, V.I. Kaydanov, and D.L. Olson: *10th CF/DRDC Meeting on Naval Applications of Materials Technology, "Thermoelectric Diagnostics for Non-Destructive Evaluation of Materials*," CRDC, Dartmouth, NS, Canada, May 13–15, 2003, pp. 648-66.
4. V.I. Kaydanov: Scientific Discussions, Colorado School of Mines, Golden, CO, 2002.
5. C. Kittel: *Introduction to Solid State Physics*, 7th ed., John Wiley & Sons, New York, NY, 1996, pp. 143-96.
6. Y. Katada, N. Washizu, and H. Baba: *Proc. Int. Conf. on High Nitrogen Steels*, Ostend, Belgium, 2004, GRIPS Media GmbH, Bad Harzburg, Germany, 2004, pp. 549-54.
7. H.F. Beeghly: *Indust. Eng. Chem.*, 1942, vol. 14 (2), pp. 137-40.
8. H.F. Beeghly: *Determination of Nitrides in Metals*, Symp. Society of Analytical Chemistry, The Iron and Steel Institute, Pittsburgh, PA, 1960, pp. 183-91.
9. J. Rawers, J. Bennett, R. Doan, and J. Siple: *Acta Metall.*, 1992, vol. 40 (6), pp. 1195-99.
10. A.N. Lasseigne, D.L. Olson, T. Boellinghaus, and V.I. Kaydanov: *Proc. QNDE Conf.*, American Institute of Physics, Golden, CO, 2004.
11. A.N. Lasseigne, D.L. Olson, T. Boellinghaus, H.J. Kleebe, and R.D. Smith: *Proc. Int. Conf. on High Nitrogen Steels*, Ostend, Belgium, 2004, pp. 577-83.
12. O. Grong: *Metallurgy Modeling of Welding*, 2nd ed., Institute of Materials, Cambridge University Press, Cambridge, United Kingdom, 1997, pp. 141-47.
13. J.A. Brooks and J.C. Lippold: *ASM Welding Handbook*, vol. 6, *Selection of Wrought Austenitic Stainless Steel*, ASM, Materials Park, OH, 1993, pp. 456-69.
14. W. Kurz and D.J. Fisher: *Fundamentals of Solidification*, Trans Tech Publishers, Aedermannsdorf, Switzerland, 1986, pp. 62-92.
15. D.L. Olson: *Welding J.*, 1985, vol. 10, pp. 281s-295s.
16. H. Wada and R.D. Pehlke: *Metall. Trans. B*, 1977, vol. 8B, pp. 675-82.
17. T. Rosenqvist: *Principles of Extractive Metallurgy*, McGraw-Hill, New York, NY, 1974, pp. 89-90.
18. L.B. Pankratz: *Thermodynamic Properties of Elements and Oxides*, U.S. Bureau of Mines Bulletin 672, U.S. Department of the Interior, Washington, DC, 1982.
19. L.B. Pankratz: *Thermodynamic Properties of Carbides, Nitrides, and Other Selected Substances*, U.S. Bureau of Mines Bulletin 695, U.S. Department of the Interior, Bureau of Mines, Washington, DC, 1995.
20. J.F. Elliot, M. Gleiser, and V. Ramakrishna: *Thermochemistry for Steelmaking*, Addison-Wesley Publishing Co., Reading, MA, 1963, vol. 2, pp. 404-05.
21. J.F. Elliot and M. Gleiser: *Thermochemistry for Steelmaking*, Addison-Wesley Publishing Co., Reading, MA, 1960, vol. 1, pp. 148-60.
22. P. Termsuksawad, S. Niyomsoan, R.B. Goldfarb, V.I. Kaydanov, D.L. Olson, B. Mishra, and Z. Gavra: *J. Alloys Compounds*, 2004, vol. 373, pp. 86-95.
23. S. Niyomsoan: Ph.D. Thesis, Colorado School of Mines, Golden, CO, 2003.